Scap is required for sterol synthesis and crypt growth in intestinal mucosa[s]

Matthew R. McFarlane,* Mary Jo Cantoria,* Albert G. Linden,* Brandon A. January,* Guosheng Liang,* and Luke J. Engelking[1],*,†

Department of Molecular Genetics* and Department of Internal Medicine,† University of Texas Southwestern Medical Center, Dallas, TX 75390-9046

Abstract SREBP cleavage-activating protein (Scap) is an endoplasmic reticulum membrane protein required for cleavage and activation of sterol regulatory element-binding proteins (SREBPs), which activate the transcription of genes in sterol and fatty acid biosynthesis. Liver-specific loss of Scap is well tolerated; hepatic synthesis of sterols and fatty acids is reduced, but mice are otherwise healthy. To determine whether Scap loss is tolerated in the intestine, we generated a mouse model (*Vil-Scap⁻*) in which tamoxifen-inducible Cre-ER^T2, a fusion protein of Cre recombinase with a mutated ligand binding domain of the human estrogen receptor, ablates Scap in intestinal mucosa. After 4 days of tamoxifen, *Vil-Scap⁻* mice succumb with a severe enteropathy and near-complete collapse of intestinal mucosa. Organoids grown ex vivo from intestinal crypts of *Vil-Scap⁻* mice are readily killed when *Scap* is deleted by 4-hydroxytamoxifen. Death is prevented when culture medium is supplemented with cholesterol and oleate.▪ These data show that, unlike the liver, the intestine requires Scap to sustain tissue integrity by maintaining the high levels of lipid synthesis necessary for proliferation of intestinal crypts.—McFarlane, M. R., M. J. Cantoria, A. G. Linden, B. A. January, G. Liang, and L. J. Engelking. **Scap is required for sterol synthesis and crypt growth in intestinal mucosa.** *J. Lipid Res.* **2015.** 56: 1560–1571.

Supplementary key words SREBP cleavage-activating protein • nuclear receptors/ sterol regulatory element-binding protein • cholesterol/biosynthesis • fatty acid/synthesis • organoid, intestine • gene expression • Niemann-Pick C1-like 1 protein

SREBP cleavage-activating protein (Scap) is an integral membrane protein that is required for the activation of sterol regulatory element-binding proteins (SREBPs), a family of membrane-bound transcription factors that activate transcription of all genes required for the synthesis of cholesterol and fatty acids (1). When cells are depleted of sterols, SREBPs are transported by Scap from endoplasmic reticulum (ER) to Golgi, where they are processed proteolytically to yield active nuclear forms. When cells are sterol-replete, Insig, an ER-resident membrane protein, binds Scap and retains the Scap-SREBP complex in the ER, thereby preventing the proteolytic activation of SREBPs (2, 3).

In cells lacking Scap, SREBP transport to the Golgi is abolished, blocking SREBP proteolysis and leading to reduced rates of de novo cholesterol and fatty acid synthesis. As a result, Scap-deficient cultured cells cannot grow without supplementation with exogenous cholesterol and fatty acids (4). The in vivo function of Scap has been explored most thoroughly in the liver, which is quantitatively the most important organ for cholesterol synthesis in most mammals (5). When *Scap* is ablated through gene knockout in rodent livers, nuclear SREBPs are not detectable, leading to reduced rates of hepatic cholesterol and fatty acid synthesis and reduced levels of cholesterol and triglycerides in the liver and plasma (6). Mice with deficiency of Scap in the liver appear phenotypically normal and have grossly normal liver function. These mice are protected from development of fatty liver and carbohydrate-induced hypertriglyceridemia, suggesting that Scap inhibition may be a potential therapeutic strategy for the treatment of nonalcoholic fatty liver disease and hyperlipidemia (7).

Determining the extrahepatic role of Scap is of interest both to elucidate the role of SREBP-mediated lipid homeostasis in extrahepatic tissues and to assess for toxicity arising from Scap inhibition in the context of the whole

Abbreviations: 4-OHT, 4-hydroxytamoxifen; ChgA, chromogranin A; CREB, cAMP response element binding protein; ER, endoplasmic reticulum; H&E, hematoxylin and eosin; HMGR, HMG-CoA reductase; IEC, intestinal epithelial cell; LGR5, leucine-rich repeat containing G protein-coupled receptor 5; MβCD, methyl-β-cyclodextrin; NGS, normal goat serum; NPC1L1, Niemann-Pick C1-like 1 protein; PAS/AB, periodic acid-Schiff-Alcian Blue; QPCR, quantitative real-time RT-PCR; Scap, SREBP cleavage-activating protein; SREBP, sterol regulatory element-binding protein; TUNEL, terminal deoxynucleotidyl transferase dUTP nick end labeling.

[1] To whom correspondence should be addressed.
  e-mail: luke.engelking@utsouthwestern.edu
[s] The online version of this article (available at http://www.jlr.org) contains supplementary data in the form of four figures, two tables, and four videos.

organism. Our prior studies investigated the role of the SREBP pathway in the intestine, which is quantitatively the second most important organ of sterol synthesis in rodents, behind the liver (5, 8). A critical role for SREBPs in the maintenance of sterol homeostasis in the intestine was suggested by our finding that ezetimibe, a cholesterol-lowering drug that blocks intestinal cholesterol uptake by inhibiting the luminal cholesterol transporter Niemann-Pick C1-like 1 protein (NPC1L1), caused major increases in intestinal nuclear SREBP-2 and HMG-CoA reductase (HMGR), the enzyme that catalyzes the rate-determining step of the sterol biosynthetic pathway (9). The activation of SREBP-2 results in a compensatory increase in cholesterol synthesis (10), which may blunt the cholesterol-lowering effect of ezetimibe. Consistent with this hypothesis is the clinical observation that the action of ezetimibe is enhanced when the drug is given with a statin, which partially blocks the compensatory increase in cholesterol synthesis (11). Statins also lead to increased nuclear SREBP-2 (12) and HMGR (13), which also tend to limit effectiveness of these drugs. These observations point to the possible utility of an intestine-specific inhibitor of SREBP-2 processing, which would prevent the compensatory increases that occur with ezetimibe and with statins.

To test this hypothesis, it was necessary to first determine whether Scap and Insig mediate normal processing and feedback inhibition of SREBPs in the intestine as they do in the liver and cultured cells. To answer these questions, we first disrupted *Insig-1* and *Insig-2* in intestinal epithelium. We observed significant increases in the amount of intestinal nuclear SREBPs and cholesterol synthesis, such that synthesis in the intestine exceeded that in liver on an organ-by-organ basis (14). Similar results were found when truncated SREBP-2 was expressed in intestinal epithelia (15). These results indicated that Insig proteins mediate feedback inhibition of cholesterol synthesis in the intestine and suggested that Scap, the binding partner for Insig, also likely plays a role in SREBP processing in the intestine.

In the current studies, we explore the in vivo role of Scap in intestine by generating and characterizing a line of mice with tamoxifen-inducible, intestine-specific deletion of *Scap*. Our data indicate that Scap-mediated cholesterol synthesis in rapidly proliferating intestinal crypts is required to maintain the integrity of the intestine.

MATERIALS AND METHODS

Generation of mice with inducible deletion of Scap in the intestine

All mice were housed in cages with 12 h light/12 h dark cycles and were maintained on a chow diet (Harlan Teklad Global Diets, Indianapolis, IN; cat. no. 7002). All animal experiments were performed with approval of the Institutional Animal Care and Research Advisory Committee at the University of Texas Southwestern Medical Center. *Vil-Scap⁻* mice were generated by intercrossing *Villin-Cre-ER^T2* transgenic mice and *Scap^flox* mice (6, 16). Tamoxifen (Sigma-Aldrich, St. Louis, MO; cat. no. T5648) was

dissolved in corn oil (Sigma-Aldrich; cat. no. C8267) at a concentration of 20 mg/ml after gently shaking at 37°C for 1 h. Doses of 0.1 ml corn oil (2 mg tamoxifen) were delivered by oral gavage once daily for up to four doses as indicated in supplementary Fig. 1.

Blood collection and cytokine measurements

Mice were euthanized with isoflurane, blood was obtained from the inferior vena cava in EDTA-coated tubes, and plasma was separated and stored at −80°C; metabolic analytes were measured as described previously (7). Plasma TNF-α was measured using a V-PLEX Pro-inflammatory Multiplex Panel (Meso Scale Discovery, Rockville, MA; cat. no. K15048D-1) read by a Meso Scale SECTOR6000 Instrument. Statistical significance was determined using the Mann-Whitney *U*-test.

Liver bacterial cultures

Livers were dissected using aseptic technique and homogenized in 10 ml sterile PBS. Diluted homogenates were grown on 5% Sheep Blood Agar (Fisher Scientific, Pittsburgh, PA; cat. no. R01200) at 37°C, and colony numbers were counted after 48 h.

Isolated intestine epithelial cell preparation

An intestinal epithelial cell (IEC) preparation was performed as described (9) with the following modifications. IECs were collected from small intestine in 20 cc of PBS with 2 mM EDTA (10 mM for colon) and 1 mM DTT. MG132 (10 μM) was added to the PBS when cell pellets were used for immunoblot analysis. After incubation at 37°C for 20 min in a metabolic shaker, tubes were vigorously shaken by hand 10 times. Cells from this isolation are a crude mixture of epithelial cells, containing both villus cells and crypt units.

Immunoblot analyses of IECs and organoids

Whole-cell extracts, membrane fractions, and nuclear extracts were prepared individually from organoids or IECs of mice, and then samples were pooled as indicated in the figure legends and subjected to SDS-PAGE and immunoblot analysis as described (9, 14). Chemiluminescence was imaged with a LI-COR Odyssey® Fc imager and quantified using LI-COR Image Studio™ software (LI-COR Biotechnology, Lincoln, NE).

Scap immunoblots were carried out with mouse monoclonal anti-Scap antibody clone 4H4 (17). SREBP-1 immunoblots were carried out with rabbit polyclonal anti-SREBP-1 IgG-211C, which was generated by immunizing rabbits with a bacterially produced (His)10-tagged protein containing amino acids 33–250 of mouse SREBP-1a. SREBP-2 immunoblots were carried out with rabbit monoclonal anti-SREBP-2 IgG-22D5, which was generated by immunizing rabbits with a bacterially produced (His)6-tagged protein containing amino acids 32–250 of mouse SREBP-2. The anti-SREBP2 hybridomas were produced and cloned using the rabbit hybridoma fusion partner 240E-1 as described (18). Other utilized antibodies included: anti-cAMP response element binding protein (CREB) (Cell Signaling, Danvers, MA; cat. no. 9197S) and anti-calnexin (Novus Biologicals, Littleon, CO; cat. no. NB100-1965), and anti-NPC1L1 (19).

Quantitative real-time RT-PCR

Total RNA was prepared from mouse tissues, IECs, or organoids and quantitative real-time RT-PCR (QPCR) was performed as described (14). Mouse *Scap exon 2* primers were 5′-CCGAG-GATGACCCTGACTGA-3′ and 5′-AGAGCAGCCCATGGTTG-TAGA-3′. Primers for mouse leucine-rich repeat containing G protein-coupled receptor 5 (LGR5) and olfactomedin 4 (OLFM1)

were obtained from Massachusetts General Hospital Primer Bank (http://pga.mgh.harvard.edu/primerbank) (20).

Histology

Tissues were fixed in 4% (v/v) paraformaldehyde in PBS, embedded in paraffin, and sectioned. Sectioning as well as hematoxylin and eosin (H&E), terminal deoxynucleotidyl transferase dUTP nick end labeling (TUNEL), and periodic acid-Schiff-Alcian Blue (PAS/AB) staining were performed by the University of Texas Southwestern-Richardson Molecular Pathology Core. For immunohistochemistry, slides were pretreated with 0.3% (v/v) hydrogen peroxide for 15 min at room temperature, followed by antigen retrieval for 10 min at 98°C in Retrievagen A buffer (BD Biosciences, San Jose, CA). The slides were then incubated for 1 h at room temperature in 10% (v/v) normal goat serum (NGS; Vector Laboratories, Burlingame, CA) in PBS, followed by overnight incubation at 4°C with the following antisera: anti-chromogranin A (ChgA) antiserum 1:400 in 10% NGS (Abcam, Cambridge, MA; cat. no. ab15160), anti-lysozyme antiserum 1:1,000 in 10% NGS (Abcam; cat. no. ab108508), anti-Ki-67 antiserum 1:400 in 10% NGS (Cell Signaling; cat. no. 12202). Slides were then incubated for 1 h at room temperature with anti-rabbit antiserum 1:500 in 10% NGS (Jackson ImmunoResearch, Westgrove, PA), followed by 60 min at room temperature in streptavidin-HRP conjugate 1:750 in 10% NGS (Life Technologies, Grand Island, NY). Activity was developed for 1 min with an AEC Substrate Kit (Life Technologies), counterstained with hematoxylin, and mounted using Aqua-Poly/Mount (Polysciences, Warrington, PA). Bright-field images of histologic sections were captured on a Leica DM2000 compound microscope, equipped with an Optronics Microfire CCD camera, using Picture-Frame 2.0 software (Optronics Inc., Goleta, CA).

Crypt isolation and culture

Crypt isolation and culture followed closely the protocol developed by Hans Clevers (21). In brief, small intestines were removed, cut open longitudinally, and placed in a 50 ml conical tube containing 30 ml ice-cold buffer consisting of PBS with 10 mM EDTA. Intestines were incubated on ice for a total of 45 min with intermittent shaking, decanting, and replacement of buffer to wash away villus elements. Semipurified crypts were then collected over 30 min with intermittent shaking, after which intestinal remnants were removed, and the crypt-containing supernatant was passed serially through cell strainers (100 µm mesh, followed by 70 µm mesh twice) to isolate crypts from larger villus debris. Thereafter, crypts were pelleted, suspended in ADMEM (Life Technologies; cat. no. 12634-010), counted under an inverted microscope, and plated to a density between 100 and 200 crypts per well in a 40 µl droplet consisting of a 1:9 ratio of ADMEM and Growth Factor-Reduced Matrigel (BD Biosciences; cat. no. 356231). Each bubble was overlaid with basic organoid media (ENR media): ADMEM containing 1 µM Jagged-1 (Anaspec, Fremont, CA; cat. no. 61298), 50 ng/ml epidermal growth factor (EGF) (R & D Systems, Minneapolis, MN; cat. no. 2028-EG-200), 500 ng/ml hR-Spondin (R & D Systems; cat. no. 4645-RS-025), 100 ng/ml Noggin (Peprotech, Rocky Hill, NJ; cat. no. 250-38), 20 ng/ml Y-27632 (Sigma-Aldrich; cat. no. Y0503-1MG), 1 µM N-acetyl cysteine (Sigma-Aldrich; cat. no. A7250-5G), 10 mM HEPES (Sigma-Aldrich; cat no. H3537), Glutamax™ (Life Technologies; cat. co. 35050-061; Stock 100×), Penicillin/Streptomycin, N2 Supplement (Life Technologies; cat. no. 17502-048), and B-27 Supplement (Life Technologies; cat. no. 12597-010).

Organoid treatment and molecular analysis

Medium was changed every 1 to 3 days depending on crypt growth. Media additions were performed as described in the figure legends at the following concentrations: 10 µM 4-hydroxy-tamoxifen (4-OHT) (Sigma-Aldrich; cat. no. H7904), 100 µM sodium oleate (Sigma-Aldrich; cat no. O7501), 50 µM cholesterol (Steraloids Inc., Newport, RI; cat no. C6760-000) solubilized in a 10 molar excess of methyl-β-cyclodextrin (MβCD) (Cyclodextrin Technologies Inc., Alachua, FL; cat no. TRMB-P). MβCD-cholesterol complexes were prepared as described (22).

For time-lapse microscopy, bright-field images of organoids were captured using a Hamamatsu ORCA-AG Camera and a Carl Zeiss 20×/0.8 NA objective. Regular bright-field microscopy of organoids was done on a Zeiss AxioObserver Z.1 microscope using a Carl Zeiss Plan-Neofluar 10×/0.30 Ph1 objective.

Organoids were harvested from matrigel by aspirating the medium and replacing it with Cell Recovery Solution (BD Biosciences; cat no. 354253), followed by incubation at 4°C for 30 min. Recovered organoids were pelleted by centrifugation at 150 g for 4 min and analyzed as described previously. Cell viability was measured using CellTiter-Glo® Luminescent Cell Viability Assay according to the manufacturer's protocol (Promega, Madison, WI; cat. no. 7572).

RESULTS

Inducible deletion of *Scap* in intestinal mucosa

Mice with floxed *Scap* alleles were bred to *Villin-Cre-ER*^{T2} transgenic mice in which Cre-ER^{T2} recombinase is driven by the gut-selective *Villin* promoter (6, 16). The resultant *Scap*$^{flox/flox}$;*Villin-Cre-ER*^{T2} transgenic mice are designated as *Vil-Scap*$^-$. The activity of Cre-ER^{T2}, a fusion protein of Cre recombinase with a mutated ligand binding domain of the human estrogen receptor, is induced by tamoxifen but not by the endogenous estrogen receptor ligand estradiol (23). Upon tamoxifen treatment, Villin-Cre-ER^{T2}-mediated deletion renders intestinal epithelia deficient in Scap. The regimen of tamoxifen dosing is shown in supplementary Fig. 1. In some experiments, tamoxifen-gavaged *Vil-Scap*$^-$ mice are compared with corn oil-gavaged *Vil-Scap*$^-$ littermates. In other experiments, littermates bearing floxed *Scap* alleles but lacking the *Villin-Cre-ER*^{T2} transgene are used as controls and are designated *Scap*^{flox} mice. Without tamoxifen treatment, *Vil-Scap*$^-$ mice were born at the expected Mendelian ratios and were grossly indistinguishable from *Scap*^{flox} littermates from birth to adulthood. These studies utilized tamoxifen-inducible Cre to study the acute effects of Scap disruption in this rapidly dividing cell population because attempts to breed mice with floxed *Scap* alleles and a constitutively active *Villin-Cre* (24) were unsuccessful, presumably owing to lethality of intestinal Scap disruption in utero.

Fig. 1 establishes a time course for Villin-Cre-ER^{T2}-mediated disruption of Scap selectively in intestinal mucosa. Tamoxifen was administered by oral gavage (supplementary Fig. 1) to *Vil-Scap*$^-$ mice, up to a maximum of four daily doses. Isolated IECs were harvested from the small intestinal mucosa in timed increments (days 1, 2, 2.5, 3, and 4) after the first dose of tamoxifen. The tamoxifen-gavaged *Vil-Scap*$^-$ mice were compared with corn oil-gavaged *Vil-Scap*$^-$ littermates, which are depicted as day 0 of tamoxifen exposure, or hereafter day 0 for simplicity. Tamoxifen caused a rapid decline in Scap mRNA as measured by QPCR.
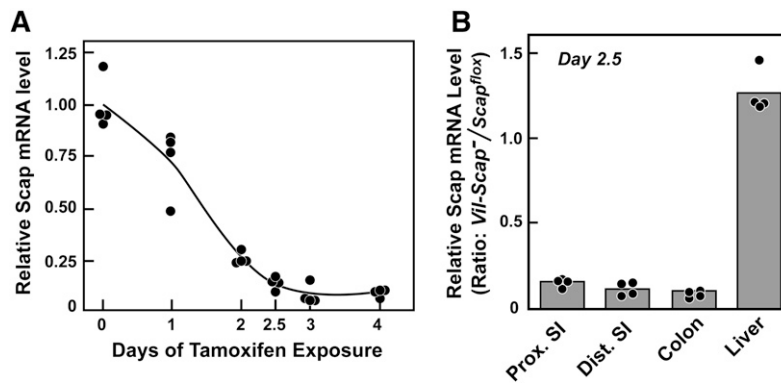
Fig. 1. Time course of inducible disruption of Scap in intestinal epithelia. A: *Scap^{flox/flox}; Villin-Cre-ER^{T2}* transgenic (*Vil-Scap^−*) mice (female, 14–17 weeks of age, four mice per time point) were orally gavaged with tamoxifen, up to a maximum of four daily doses, as shown in supplementary Fig. 1. Small intestines were harvested without tamoxifen dosage (0 days of tamoxifen exposure), or at 1, 2, 2.5, 3, or 4 days after the initial dose of tamoxifen. Total RNA was prepared from isolated IECs, and Scap mRNA was measured by QPCR using cyclophilin as the invariant control. The mean mRNA value at day 0 is arbitrarily defined as 1.0. Filled circles indicate the value of individual mice, and the black line indicates the mean. B: *Scap^{flox}* and *Vil-Scap^−* mice (female, 14–15 weeks of age, four per group) were administered three doses of tamoxifen, and then tissues were collected at day 2.5 after the initial dose. Total RNA was isolated from liver and from IECs from proximal small intestine (Prox. SI), distal small intestine (Dist. SI), and colon. Scap mRNA was measured by QPCR as described in A. The fold expression in *Vil-Scap^−* tissues is expressed as the ratio of Scap mRNA values of *Vil-Scap^−* to *Scap^{flox}* mice, which were arbitrarily defined as 1.0. Bars indicate the mean of four mice per tissue.

Compared with day 0, Scap mRNA decreased by 27% on day 1, 86% on day 2.5, and 91% on day 4 (Fig. 1A). To examine the extent of Scap disruption more broadly in the gastrointestinal system, Scap mRNA was measured in liver and in IECs from proximal small intestine, distal small intestine, and colon from *Scap^{flox}* and *Vil-Scap^−* mice at day 2.5 after the first dose of tamoxifen. Day 2.5 was selected because the reduction in Scap expression was nearly maximal at day 2.5 (Fig. 1A), while intestinal morphology remained normal (supplementary Fig. 2). As expected, ligand activation of Cre-ER^{T2} in *Vil-Scap^−* mice did not alter Scap mRNA in the liver, whereas Scap mRNA was reduced by 85% to 92% in segments of large and small intestine compared with *Scap^{flox}* controls (Fig. 1B). We subsequently focused on the small intestine rather than the colon because the histological changes at day 4 were much more pronounced in the small intestine than in the colon (supplementary Fig. 2).

Intestinal Scap disruption provokes a severe enteropathy

The *Vil-Scap^−* mice were normal in appearance and behavior for day 0 through day 3. On day 4 after tamoxifen initiation, they became moribund and were euthanized. Every *Vil-Scap^−* mouse lost weight by day 4; a mean weight loss of 12% between day 3 and day 4 was observed (**Fig. 2A**). On day 4, *Vil-Scap^−* mice were hunched, less responsive to stimuli, and developed liquid stools. *Scap^{flox}* littermates experienced no change in body weight or change in appearance, behavior, or stool form throughout the experiment. On gross inspection in situ, the intestines of *Vil-Scap^−* mice were fluid filled (Fig. 2B). When excised and uncoiled, the intestinal length (duodenum to rectum) was shortened by 21% compared with *Scap^{flox}* littermates (Fig. 2C), indicating a reduction in tissue elasticity suggestive of tissue injury. Stomachs of the *Vil-Scap^−* mice were distended with partially digested

food, implying impairment in stomach emptying, while the remainder of small intestine and colon lumen was filled with fluid. In contrast, stomachs of the *Scap^{flox}* mice contained a moderate amount of partially digested food, chyme was present in the small intestine, and stool was present in the colon.

The gross appearance of the gastrointestinal tract suggests that poor nutrition and fluid losses may explain, in part, the condition of the *Vil-Scap^−* mice on day 4. In addition, because intestinal injuries can become complicated by bacteremia as the intestinal barrier function fails, we suspected that bacteremia and a systemic inflammatory response could also result in the rapid decline of the *Vil-Scap^−* mice on day 4. Accordingly, we measured plasma TNF-α levels and quantitative liver bacterial counts from *Scap^{flox}* and *Vil-Scap^−* mice on day 4. TNF-α is released from macrophages in response to a variety of stimuli, including endotoxin (25), and is elevated in other murine models of intestinal injury such as dextran-sodium sulfate-induced colitis (26). Plasma TNF-α levels were 20-fold higher in *Vil-Scap^−* compared with *Scap^{flox}* mice (31 ± 9 vs. 1.5 ± 0.1 pg/ml, mean ± SEM, $P < 0.0001$ by Mann-Whitney *U*-test). Homogenates of liver from 3 of 12 *Vil-Scap^−* mice plated onto blood agar media grew bacterial colonies (mean colony forming units (CFU) per liver of 2.5×10^3), compared with 0 of 12 *Scap^{flox}* mice.

Fig. 3 shows histological and immunohistochemical analysis of mid-small intestine from *Vil-Scap^−* mice on days 0, 3, and 4. On day 3, *Vil-Scap^−* mice had lost 1% of their body weight (Fig. 2A) but otherwise appeared grossly normal. At this time point, H&E and TUNEL staining revealed a small increase in apoptotic cells in the crypts, but the villi appeared normal.

The most abundant cells of the intestinal villus-crypt unit are villus enterocytes and proliferating precursor cells of the crypt, which can be followed by the marker Ki67 (27). In addition, far less numerous differentiated cells
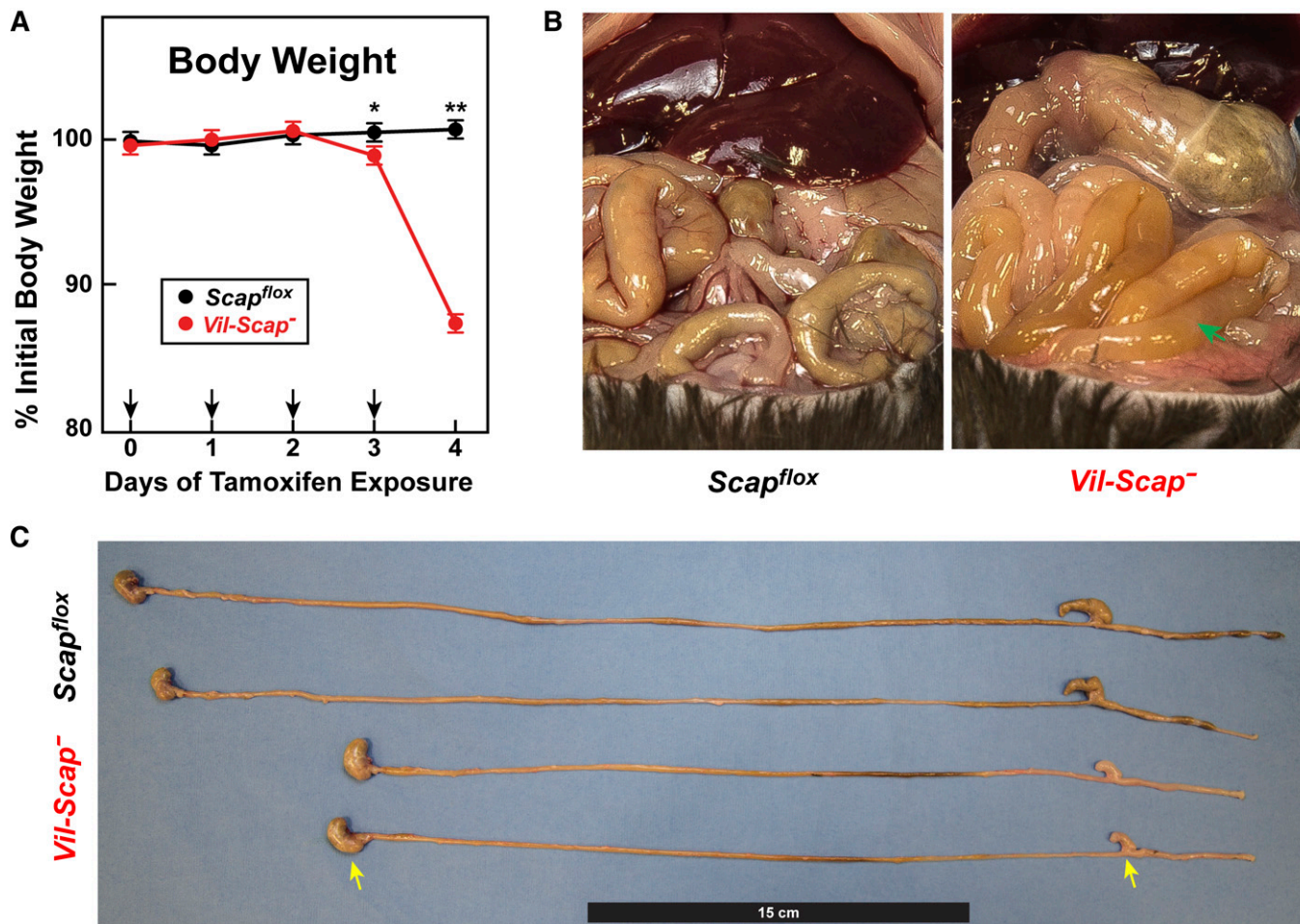
Fig. 2. Disruption of intestinal Scap rapidly produces a severe enteropathy. A: *Scap^flox* and *Vil-Scap^−* mice (male, 10–12 weeks of age, 10 mice per group) were administered tamoxifen once daily for four doses as indicated by black arrows. Mice were euthanized and dissected on day 4 after the initial dose of tamoxifen and body weights measured. B, C: Gross appearance of viscera in situ and dissected gastrointestinal tracts from *Scap^flox* and *Vil-Scap^−* are shown. A green arrow indicates a fluid-filled small intestine. Yellow arrows indicate a dilated, food-filled stomach and shrunken, fluid-filled appendix. Statistical significance was assessed by the two-tailed Student's *t*-test (A). * $P < 0.05$; ** $P < 0.001$.

types are present: tuft cells, goblet cells, enteroendocrine cells, and Paneth cells. We assessed these latter three cell types by staining with PAS/AB (goblet cells and Paneth cells) or antibodies against ChgA (enteroendocrine cells) and lysozyme (Paneth cells). On day 3, the numbers of PAS/AB$^+$, Ki-67$^+$, ChgA$^+$, and lysozyme$^+$ cells appeared largely unchanged from day 0.

On day 4, H&E stain revealed necrosis throughout the epithelium, with a near-complete collapse of villi and effacement of crypts. The number of Ki67$^+$ cells in the crypts was dramatically reduced. Scattered Ki67$^+$ cells in the residual villi corresponded to infiltrating inflammatory cells (mostly marginating neutrophils) in the lamina propria. Goblet cells were no longer clearly distinguished with PAS/AB staining. Rare ChgA$^+$ cells remained; lysozyme was found in sloughed epithelial elements in the lumen but was depleted in the crypt base, suggesting Paneth cell degranulation or loss. Strong TUNEL signal was seen in residual crypt structures, overlapping the area in which Ki67 signal was lost.

Taken together, the findings of Figs. 1–3 demonstrate that Villin-Cre-ER^{T2}-mediated recombination nearly ablates Scap expression in intestinal mucosa by day 2.5 after

ligand administration, and this loss is followed on day 4 by an acute, severe enteropathy characterized by loose stools, weight loss, and sepsis. Inasmuch as the primary function of Scap is to mediate the proteolytic processing of SREBPs in order to drive cholesterol and fatty acid synthesis, we then asked whether the loss of Scap in the intestinal mucosa is associated with reductions in intestinal SREBP proteolysis and lipid synthesis, and whether these reductions occur prior to the onset of overt intestinal injury at day 4.

Intestinal Scap required for SREBP-mediated mucosal lipid synthesis

In **Fig. 4**, we measured proteolytic processing of SREBPs and the expression of genes required for the synthesis of fatty acids and cholesterol whose transcription is stimulated by SREBPs. Total RNA, membrane fractions, and nuclear extracts of IECs were prepared from *Scap^flox* and *Vil-Scap^−* mice treated with either corn oil or tamoxifen and harvested at day 2.5. Scap mRNA as measured by QPCR was decreased by 90% in IECs from tamoxifen-treated *Vil-Scap^−* mice compared with tamoxifen-treated *Scap^flox* mice (Fig. 4B). Scap mRNA was not decreased in *Vil-Scap^−* mice that
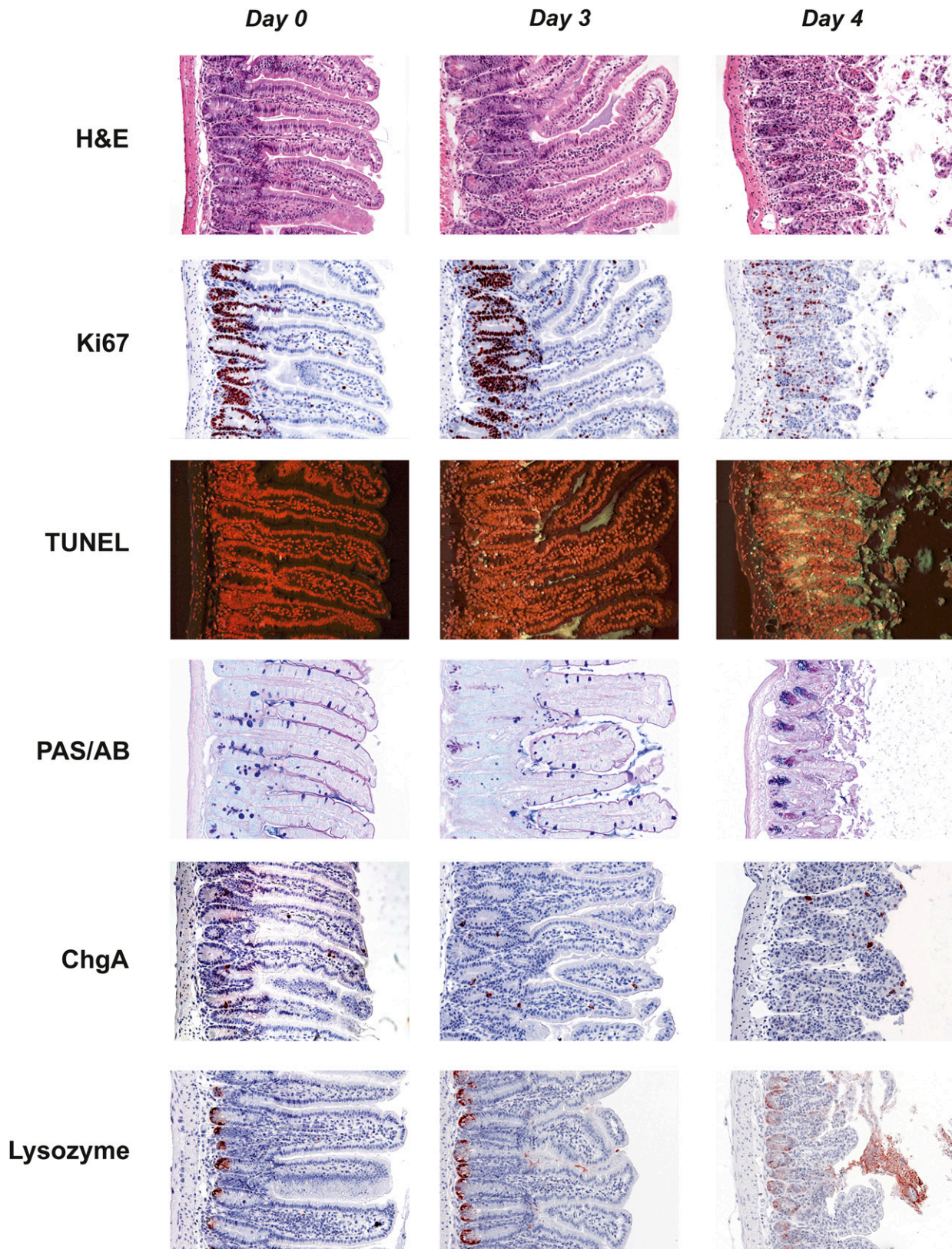
Fig. 3. Destruction of villus and crypt structures in *Vil-Scap*⁻ mice. Representative histologic sections of mid-small intestine from 8-week-old male *Vil-Scap*⁻ mice that were administered tamoxifen as described in supplementary Fig. 1. Intestines were harvested on day 0 (without tamoxifen administration) or on day 3 or 4 after the initial dose of tamoxifen. Magnification, 20×.

received corn oil vehicle (data not shown). Corresponding with the fall in Scap, nuclear SREBP-1 and SREBP-2 were markedly decreased in the tamoxifen-treated *Vil-Scap*⁻ mice compared with the other groups (Fig. 4A, lane 3 vs. lanes 1 and 2). Levels of the luminal cholesterol transporter (NPC1L1), a control membrane protein (calnexin), and a control nuclear protein (CREB), were not significantly different between the three groups of mice.
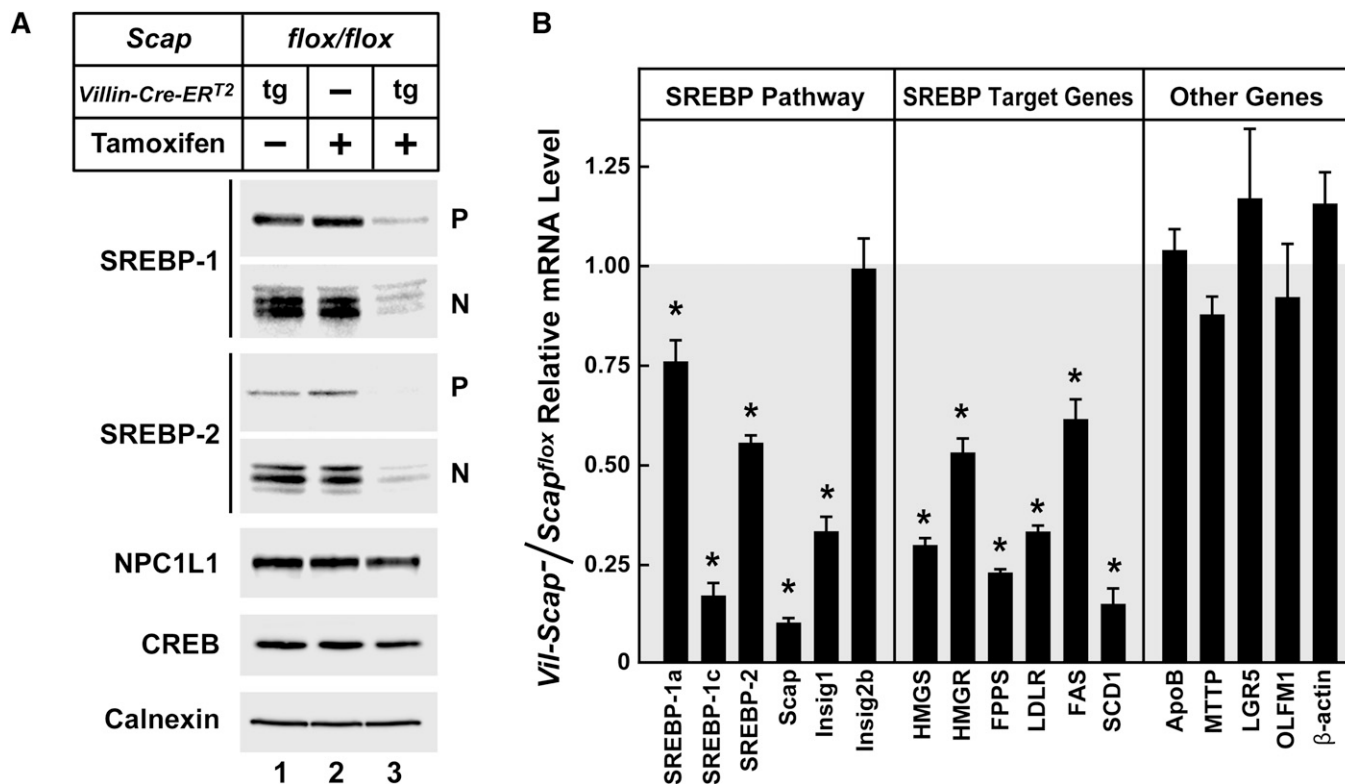
Fig. 4. Diminished SREBP processing in Scap-deficient small intestine. *Scap^flox* and *Vil-Scap^−* mice (male, 14–18 weeks of age, six mice per group) were administered three doses of corn oil vehicle or tamoxifen, and tissues were collected at day 2.5 after the initial dose of tamoxifen (supplementary Fig. 1). A: Immunoblot analysis. IECs were fractionated, and equal amounts of protein from each mouse were pooled; aliquots of the pooled membranes (75 μg) and nuclear extract (50 μg) were subjected to SDS-PAGE and immunoblot analysis. The precursor and nuclear forms of SREBPs are denoted as P and N, respectively. Immunoblots of CREB and calnexin were used as loading controls for the nuclear extract and membrane fractions, respectively. B: Relative mRNA levels in tamoxifen-dosed control and *Vil-Scap^−* mice (the same mice as in lanes 2 and 3 in A). Total RNA from IECs was separately isolated; equal amounts of RNA from each mouse were pooled and subjected to QPCR. Each value represents the mean ± SEM of data from six *Vil-Scap^−* mice relative to that of *Scap^flox* mice, which was arbitrarily defined as 1.0. * $P < 0.01$ denotes the level of statistical significance (two-tailed Student's *t*-test) between *Scap^flox* and *Vil-Scap^−* mice. Tg, transgenic.

Fig. 4B shows mRNA levels as measured by QPCR from the *Vil-Scap^−* mice used in Fig. 4A (lanes 2 and 3). Consistent with the fall in nuclear SREBP-1 and SREBP-2, the mRNAs for SREBPs and their transcriptional targets were reduced. Transcription of SREBPs is known to be regulated by nuclear SREBPs in a feed-forward fashion (28, 29). Accordingly, the mRNA levels of SREBP-1a, SREBP-1c, and SREBP-2 were decreased by 24%, 83%, and 45%, respectively, in tamoxifen-treated *Vil-Scap^−* mice compared with *Scap^flox* controls. mRNAs involved in fatty acid synthesis such as FAS and stearoyl-CoA desaturase 1 were decreased by 39% and 85%, respectively. Four mRNAs involved in sterol biosynthesis or LDL uptake [HMG-CoA synthase (HMGS), HMGR, farnesyl pyrophosphate synthase, and LDL receptor (LDLR)] were decreased by 47% to 77%. The expression of other lipid-related genes such as apoB and microsomal triglyceride transfer protein, markers of crypt stem cells (LGR5 and OLFM1), and a housekeeping gene (β-actin) was unchanged in *Vil-Scap^−* mice.

To test the whether the loss of Scap and nuclear SREBPs affects intestinal lipid synthesis in vivo, we measured the incorporation of intraperitoneally injected ³H-labeled water into digitonin-precipitable sterols and fatty acids in *Scap^flox* and *Vil-Scap^−* mice at day 2.5. In the *Vil-Scap^−* mice,

sterol synthesis was decreased by 37% and 54% in proximal and distal small intestine, respectively (**Fig. 5A**). In contrast, fatty acid synthesis was reduced only in the distal small intestine (Fig. 5B). These data concur with the prior findings that SREBP-2 is more abundant in the ileum than in the proximal small intestine (9, 30). Sterol and fatty acid synthesis rates were not significantly altered in colon or spleen. Despite the fall in sterol biosynthetic rate, the total cholesterol content in small intestine IECs was no different in *Scap^flox* and *Vil-Scap^−* mice at day 2.5 (supplementary Table 2). This finding does not rule out the possibility that the cholesterol content of certain population(s) of IECs decline in accordance with the fall in sterol synthesis in the *Vil-Scap^−* mice.

Exogenous lipids prevent crypt growth failure in Scap-deficient intestinal organoids

Inasmuch as cell proliferation is dependent on sterol and isoprenoid supply (31) and because Scap (supplementary Fig. 3), SREBP-2 abundance (9, 32), and sterol synthesis (33, 34) are all enriched in proliferating intestinal crypts relative to the upper villi, we hypothesized that the severe intestinal toxicity seen on day 4 is being driven by a loss of cell proliferation in the crypts. To test this hypothesis in
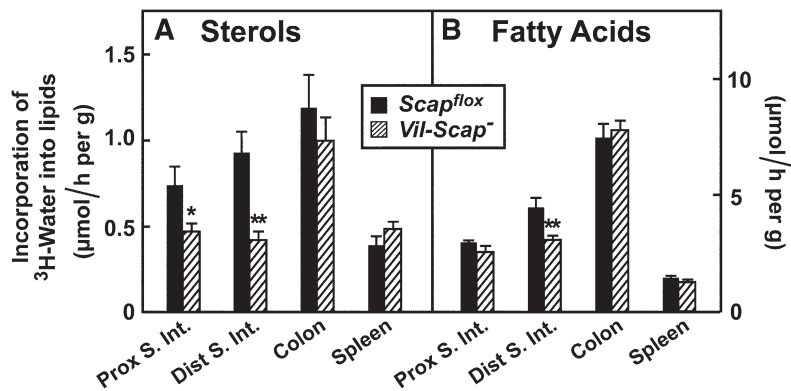
Fig. 5. Decreased sterol synthesis in Scap-deficient small intestine. *Scap^flox* and *Vil-Scap^−* mice (male, 11–12 weeks of age, seven per group) were administered tamoxifen as described in Fig. 4. On day 2.5, mice were injected intraperitoneally with ³H-labeled water (50 mCi in 0.2 ml of saline). One hour later, tissues were removed and digitonin-precipitable sterols (A) or fatty acids (B) were isolated and subjected to scintillation counting. The small intestine was divided into two segments of equal length, proximal (Prox. S. Int.) and distal (Dist. S. Int.). Each bar represents mean ± SEM of data from seven mice. * $P < 0.05$, ** $P < 0.01$ denotes the level of statistical significance (two-tailed Student's *t*-test) between *Scap^flox* and *Vil-Scap^−* mice.

vivo, we attempted to prevent the intestinal injury in tamoxifen-dosed *Vil-Scap^−* mice by administering a variety of exogenously supplied sterols and fats, without success (data not shown). Suspecting that our inability to rescue *Vil-Scap^−* animals was due to our inability to deliver high doses of cholesterol to crypt cells in vivo, we turned to the recently developed intestinal organoid system of Sato et al. (21) for ex vivo testing of cell proliferation in isolated crypts.

Crypt units were isolated, embedded in matrigel, and grown in basic organoid medium for 4 days, after which 4-OHT, sodium oleate, and cholesterol complexed to MβCD (MβCD-cholesterol) were added to the culture media as indicated. Organoids were then grown until the seventh day after isolation and photographed (**Fig. 6A**). Cell viability was measured by ATP bioluminescence assay (35), in which luciferin is oxidized in an ATP-dependent

fashion by firefly luciferase to produce luminescence (Fig. 6B). As described by Sato et al. (21), organoids grown in basic media without 4-OHT (Fig. 6A, panels 1–4) formed complex structures with multiple budding protrusions surrounding a dense core of apoptotic cells. The addition of lipids had no effect. 4-OHT, the active metabolite of tamoxifen, stimulates Cre-ER^T2 to induce Scap disruption ex vivo, and killed the organoids completely, leaving only clumps of debris (Fig. 6A, panel 5) with nearly undetectable ATP, confirming an absence of viable cells. 4-OHT-mediated organoid killing was prevented by the addition of cholesterol plus oleate (Fig. 6A, panel 8). In cells that received cholesterol plus oleate, 4-OHT caused no decrease in ATP (Fig. 6B). Oleate alone did not rescue the cells (Fig. 6A, panel 7). Cholesterol alone preserved ATP levels, but the organoids had
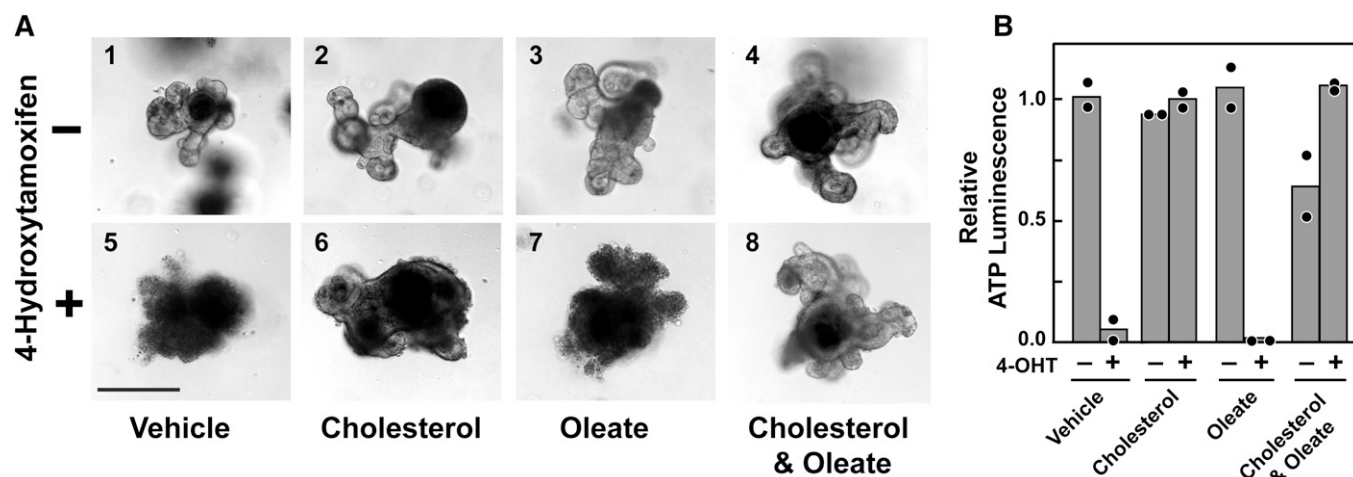

Fig. 6. Scap-deficient small intestinal organoids are nonviable unless cultured with cholesterol and oleate. Intestinal crypts from three *Vil-Scap^−* mice were isolated, embedded in matrigel, and cultured in independent experiments. Data from the crypts of one mouse are shown in A and from two mice in B. Organoids were grown for 4 days, at which time the wells were supplemented with 10 μM 4-OHT, 50 μM MβCD-cholesterol, and/or 100 μM oleate as indicated. Organoids not receiving MβCD-cholesterol or 4-OHT received an equal concentration of vehicle (MβCD and/or ethanol, respectively). A: Representative organoids imaged under bright-field microscopy (magnification, 10×) on the seventh day in culture. Bar indicates 200 μm. B: Cell viability was measured by ATP luminescence on the eighth day in culture. Filled circles indicate the values from two independent experiments; gray bars indicate the mean. The mean value of organoids not receiving 4-OHT or lipid supplements is arbitrarily defined as 1.0.

an abnormal appearance lacking budding protrusions (Fig. 6A, panel 6). Preliminary experiments were also performed to assess whether 4-OHT affected the growth of cultured organoids absent complete Scap disruption. The growth and morphology of organoids from a $Scap^{flox/+};Villin-Cre-ER^{T2}$ transgenic mouse, which retain one intact allele of $Scap$ after Cre-mediated recombination, was not affected by the addition of 4-OHT to the culture medium (data not shown).

Considered together, these data indicate that Scap-deficient organoids require exogenous cholesterol plus an unsaturated fatty acid to maintain viability and normal morphology. These data are similar to observations in Chinese hamster ovary (CHO) cells lacking nuclear SREBPs, owing to inactivating mutations in Scap, site-1 protease, or site-2 protease that require cholesterol plus an unsaturated fatty acid for growth (4, 36, 37). Other agents were unable to rescue growth in Scap-deficient organoids, including cholesterol solubilized in ethanol, β-VLDL, farnesol, geranylgeraniol, and others (data not shown). Whether other classes of lipids, such as saturated fatty acids, phospholipids, sphingolipids, or others modulate the growth of Scap-deficient organoids remains an open question.

Time-lapse images from representative individual $Vil-Scap^-$ organoids grown with or without 4-OHT and cholesterol plus oleate are shown in **Fig. 7**. The full videos can be viewed online (supplementary Videos 1–4). Scap-deficient 4-OHT-treated organoids that did not receive lipid supplementation collapsed at ∼24 h, while organoids that received cholesterol plus oleate proliferated throughout the time-lapse period.

The experiment in **Fig. 8** was performed to follow the time course of cell death after elimination of Scap from the organoid culture. 4-OHT was added to organoids either 1.5 or 3 days prior to harvest on the eighth day in culture. After 1.5 days of 4-OHT exposure, the amount of Scap had declined markedly as determined by immunoblotting, and there was no difference when cholesterol plus oleate were present (Fig. 8A). At this time point, we still detected nuclear SREBP-1 and SREBP-2, and the amounts were reduced in the presence of lipids, as expected from previous knowledge that cholesterol, and to a lesser extent unsaturated fatty acids, block proteolytic processing of SREBPs (38–40). By 3 days of 4-OHT treatment, Scap was undetectable in the absence or presence of cholesterol plus oleate, indicating that gene knockout was complete.
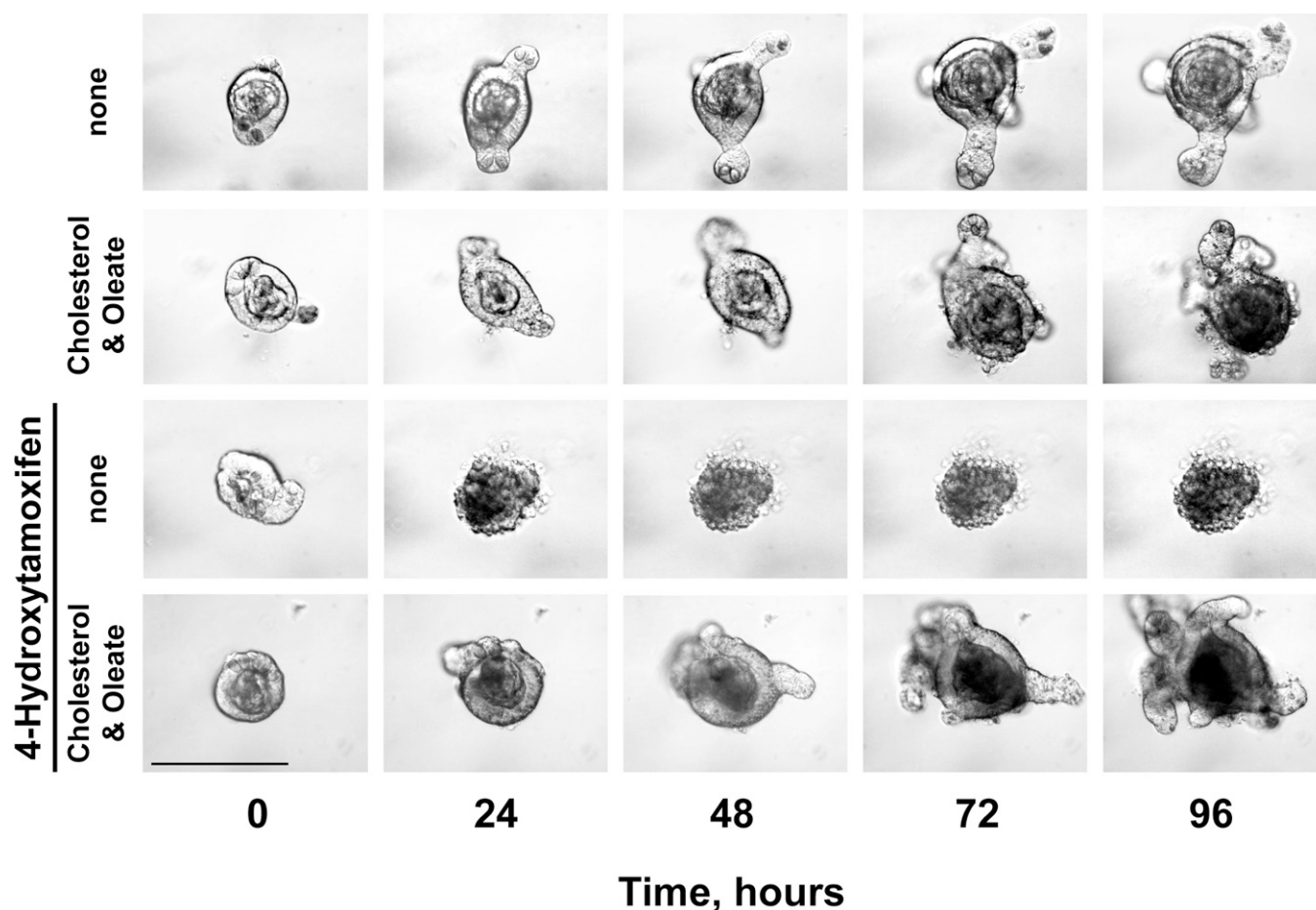

Fig. 7. Time-lapse imaging of Scap-deficient organoids. Intestinal crypts from a $Vil-Scap^-$ mouse were isolated, matrigel-embedded, and grown for 4 days, when lipids and 4-OHT were added as described in Fig. 6. Single organoids were visualized under bright-field microscopy (magnification, 20×) and photographed every 20 min for the following 96 h. Time-lapse videos can be seen in supplementary Videos 1–4. Still images taken every 24 h from the time-lapse sequences are shown. Bar indicates 200 μm.
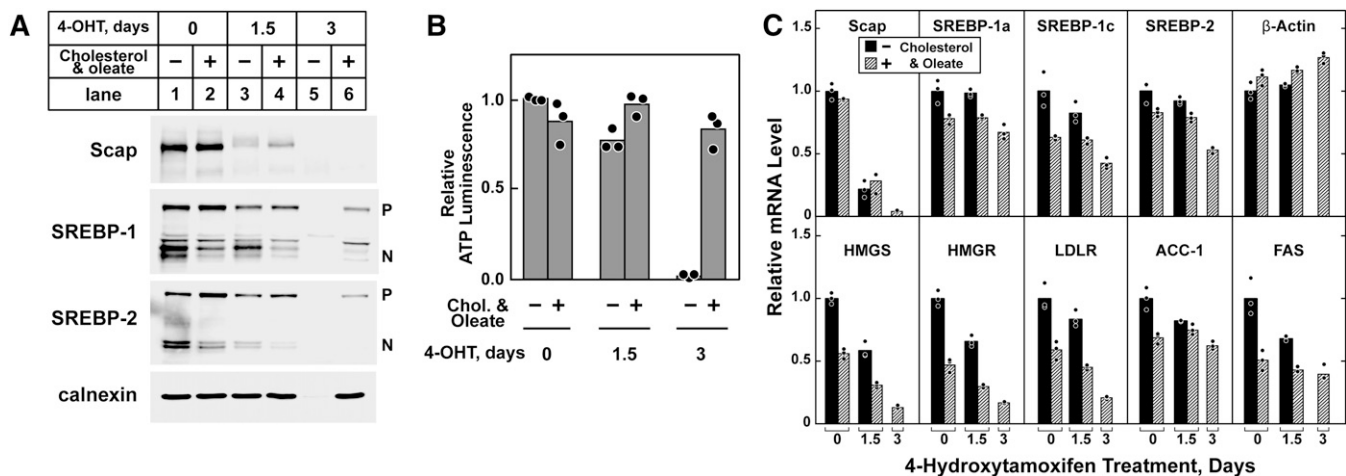
Fig. 8. Cholesterol suppresses SREBP processing and obviates nuclear SREBP requirement in Scap-deficient organoids. Intestinal crypts from three *Vil-Scap⁻* mice were separately isolated, embedded in matrigel, and grown for 5 days, at which time half of the wells were supplemented with 50 μM MβCD-cholesterol and 100 μM oleate. 4-OHT (10 μM) was then added, and organoids were harvested 1.5 or 3 days later. Wells not receiving 4-OHT instead received ethanol vehicle and are indicated (0 days 4-OHT). Organoids were recovered from matrigel on the eighth day in culture. A: Immunoblot analysis. Organoids from five wells per mouse were pooled, and whole-cell extracts prepared. Aliquots of pooled protein (45 μg) were subjected to SDS-PAGE and immunoblot analysis. The precursor and nuclear forms of SREBPs are denoted as P and N, respectively. Immunoblot of calnexin was used as a loading control. B: Cell viability as estimated by ATP luminescence. C: Relative mRNA levels. Organoids from five wells per mouse were pooled, and total RNA was isolated and subjected to QPCR using cyclophilin as the invariant control. In B and C, filled circles indicate the value of organoids from each individual mouse, and bars indicate the mean value. Values from organoids receiving neither 4-OHT nor MβCD-cholesterol plus oleate were arbitrarily defined as 1.0. QPCR data from organoids that received 4-OHT for 3 days without lipid supplementation are not shown, as no RNA was recovered.

In the absence of added lipids, organoids appeared nonviable (data not shown), and we detected no precursor or nuclear forms of SREBPs. We were also unable to detect calnexin, a cellular housekeeping protein, consistent with the disappearance of viable cells. In the presence of cholesterol plus oleate on day 3, we found normal levels of calnexin. Nuclear SREBP-1 was reduced but detectable. Nuclear SREBP-2 was absent, again consistent with the cholesterol-mediated inhibition of SREBP processing.

Fig. 8B shows the cellular ATP levels as measured by luminescence assay. In the absence of added lipids, ATP levels were maintained after 1.5 days of 4-OHT treatment. After 3 days, ATP was undetectable in the absence of added lipids but was maintained at normal levels in the presence of cholesterol plus oleate. Fig. 8C shows mRNA levels of SREBP target genes as measured by QPCR. mRNAs encoding HMGS, HMGR, and the LDLR declined roughly in parallel with the decline in nuclear SREBP-2. The decline in fatty acid synthesizing genes acetyl-CoA carboxylase and FAS was clear but less pronounced than in the cholesterol-related genes. After 3 days of 4-OHT treatment, we were unable to detect any mRNAs in the organoids that were incubated in the absence of exogenous lipids.

DISCUSSION

The intestine and liver form a central homeostatic feedback loop for cholesterol: hepatic cholesterol is secreted in bile and reaches the intestinal lumen, where it suppresses intestinal cholesterol synthesis when it is reabsorbed into epithelial cells. Sterols synthesized de novo or absorbed in the intestine are packaged into lipoproteins and ultimately reach the liver via the plasma, where they mediate feedback inhibition of hepatic sterol synthesis. The current study, taken together with our prior studies in the liver and small intestine (14, 41), demonstrates that Scap/Insig-mediated sterol sensing imparts cell-autonomous feedback regulation on SREBPs in hepatocytes and in small IECs to balance cholesterol flux between the liver and the small intestine.

In addition to this homeostatic function, which occurs primarily in villus enterocytes of the proximal small intestine that express NPC1L1 and are the predominant site of sterol absorption (42), the current study demonstrates that nuclear SREBPs maintain mucosal integrity by driving de novo lipid synthesis in the intestinal crypt cells throughout the intestine. Unlike villus cells, which under sterol-replete conditions express SREBPs modestly, crypt cells have abundant Scap and SREBPs (supplementary Fig. 3; Refs. 9, 31). Intestinal crypts require high sterol biosynthetic rates to maintain membrane production for cell proliferation (43). In mice and humans, the surface area of the intestine is 10- to 100-fold greater than that of the skin, and these intestinal mucosal cells turn over every 3–5 days (44, 45). Prior to the current studies, it was unclear whether SREBPs are needed to drive lipid production or whether lipids absorbed from the intestinal lumen would be sufficient to maintain cell growth and maturation. Here, we show that Scap is required for the maintenance of the intestinal mucosa and that its essential function in this context is to support de novo sterol synthesis in intestinal crypts by promoting SREBP proteolysis. Indeed, the data in Fig. 8 show that Scap-deficient intestinal crypts survive only when the end product of SREBP action (namely,

cholesterol) accumulates to levels at which it suppresses SREBP proteolysis.

These data do not answer whether Scap and SREBPs coordinate sterol synthesis and sterol absorption in the intestine. Inasmuch as NPC1L1 expression is intact at day 2.5 (Fig. 4A), sterol absorption in villus enterocytes of the *Vil-Scap*⁻ mice is likely intact until this time point; however, the acuity with which *Vil-Scap*⁻ mice decline from day 2.5 to day 4 precludes our ability to accurately measure sterol absorption in this model.

In addition to the current experiments with intestine-specific *Villin-Cre-ER*^{T2}, we performed other experiments in which we disrupted Scap using the ubiquitously expressed *Ubc-Cre-ER*^{T2} (46). The results were nearly identical (supplementary Fig. 4). Tamoxifen-dosed *Scap*$^{flox/flox}$; *Ubc-Cre-ER*^{T2} transgenic mice exhibited nonrecoverable weight loss, loose stools, and intestinal epithelial destruction over a 5-day period, suggesting that the intestinal mucosa is particularly sensitive to perturbation of Scap.

In contrast to the intestine, the liver is able to tolerate loss of Scap. In liver-specific Scap knockouts, liver size and histology are normal (6, 7), suggesting that Scap may not be required for maintenance of organs that have a slower cellular proliferation rate under normal circumstances. Whether Scap and SREBPs are needed for liver regeneration after injury, when cell proliferation accelerates, is an open question. Studies in humans and rodents suggest that SREBP-1c is upregulated in alcoholic and nonalcoholic fatty liver disease (47–49), where it is thought to drive pathological triglyceride accumulation. As such, inhibiting SREBP-1c, either directly or indirectly by targeting Scap, could block the synthesis of excess triglyceride and thereby be a therapeutic strategy in fatty liver disease or hypertriglyceridemia. The current studies confirm an essential requirement for Scap in proliferating cells in vivo and point to potential gastrointestinal toxicity of Scap-directed therapies developed for clinical use.

The organoid culture system of Sato et al. (21), which was used in this study, has revolutionized the study of epithelial stem cell biology, including the identification of the *Lgr5*⁺ crypt base cells and their interaction with Paneth cells as the intestinal stem cell niche (50). The current study does not identify which cell populations in the crypt are most reliant on Scap for growth; we previously found neutral lipid accumulation in the crypt bases of mice with intestine-specific *Insig* disruption (14), which could suggest a possible role for Scap/Insig sterol regulation in Paneth cells or stem cells that compose the crypt base. Future studies will be necessary to precisely determine which cell population(s) in the crypts are most dependent on SREBPs, potentially unraveling details of the function of the SREBP pathway and more largely of lipid biology in adult stem cells. ⏷

REFERENCES

1. Horton, J. D., J. L. Goldstein, and M. S. Brown. 2002. SREBPs: activators of the complete program of cholesterol and fatty acid synthesis in the liver. *J. Clin. Invest.* **109:** 1125–1131.
2. Yang, T., P. J. Espenshade, M. E. Wright, D. Yabe, Y. Gong, R. Aebersold, J. L. Goldstein, and M. S. Brown. 2002. Crucial step in cholesterol homeostasis: Sterols promote binding of SCAP to INSIG-1, a membrane protein that facilitates retention of SREBPs in ER. *Cell.* **110:** 489–500.
3. Ye, J., and R. A. DeBose-Boyd. 2011. Regulation of cholesterol and fatty acid synthesis. *Cold Spring Harb. Perspect. Biol.* **3:** a004754.
4. Rawson, R. B., R. DeBose-Boyd, J. L. Goldstein, and M. S. Brown. 1999. Failure to cleave sterol regulatory element-binding proteins (SREBPs) causes cholesterol auxotrophy in Chinese hamster ovary cells with genetic absence of SREBP cleavage-activating protein. *J. Biol. Chem.* **274:** 28549–28556.
5. Spady, D. K., and J. M. Dietschy. 1983. Sterol synthesis in vivo in 18 tissues of the squirrel monkey, guinea pig, rabbit, hamster, and rat. *J. Lipid Res.* **24:** 303–315.
6. Matsuda, M., B. S. Korn, R. E. Hammer, Y. A. Moon, R. Komuro, J. D. Horton, J. L. Goldstein, M. S. Brown, and I. Shimomura. 2001. SREBP cleavage-activating protein (SCAP) is required for increased lipid synthesis in liver induced by cholesterol deprivation and insulin elevation. *Genes Dev.* **15:** 1206–1216.
7. Moon, Y. A., G. Liang, X. Xie, M. Frank-Kamenetsky, K. Fitzgerald, V. Koteliansky, M. S. Brown, J. L. Goldstein, and J. D. Horton. 2012. The Scap/SREBP pathway is essential for developing diabetic fatty liver and carbohydrate-induced hypertriglyceridemia in animals. *Cell Metab.* **15:** 240–246.
8. Xie, C., S. D. Turley, and J. M. Dietschy. 2009. ABCA1 plays no role in the centripetal movement of cholesterol from peripheral tissues to the liver and intestine in the mouse. *J. Lipid Res.* **50:** 1316–1329.
9. Engelking, L. J., M. R. McFarlane, C. K. Li, and G. Liang. 2012. Blockade of cholesterol absorption by ezetimibe reveals a complex homeostatic network in enterocytes. *J. Lipid Res.* **53:** 1359–1368.
10. Repa, J. J., S. D. Turley, G. Quan, and J. M. Dietschy. 2005. Delineation of molecular changes in intrahepatic cholesterol metabolism resulting from diminished cholesterol absorption. *J. Lipid Res.* **46:** 779–789.
11. Turley, S. D., and J. M. Dietschy. 2003. The intestinal absorption of biliary and dietary cholesterol as a drug target for lowering the plasma cholesterol level. *Prev. Cardiol.* **6:** 29–33, 64.
12. Sheng, Z., H. Otani, M. S. Brown, and J. L. Goldstein. 1995. Independent regulation of sterol regulatory element-binding proteins 1 and 2 in hamster liver. *Proc. Natl. Acad. Sci. USA.* **92:** 935–938.
13. Kita, T., M. S. Brown, and J. L. Goldstein. 1980. Feedback regulation of 3-hydroxy-3-methylglutaryl coenzyme A reductase in livers of mice treated with mevinolin, a competitive inhibitor of the reductase. *J. Clin. Invest.* **66:** 1094–1100.
14. McFarlane, M. R., G. Liang, and L. J. Engelking. 2014. Insig proteins mediate feedback inhibition of cholesterol synthesis in the intestine. *J. Biol. Chem.* **289:** 2148–2156.
15. Ma, K., P. Malhotra, V. Soni, O. Hedroug, F. Annaba, A. Dudeja, L. Shen, J. R. Turner, E. A. Khramtsova, S. Saksena, et al. 2014. Overactivation of intestinal SREBP2 in mice increases serum cholesterol. *PLoS ONE.* **9:** e84221.

16. el Marjou, F., K. P. Janssen, B. H. Chang, M. Li, V. Hindie, L. Chan, D. Louvard, P. Chambon, D. Metzger, and S. Robine. 2004. Tissue-specific and inducible Cre-mediated recombination in the gut epithelium. *Genesis.* **39:** 186–193.

17. Ikeda, Y., G. N. Demartino, M. S. Brown, J. N. Lee, J. L. Goldstein, and J. Ye. 2009. Regulated endoplasmic reticulum-associated degradation of a polytopic protein: p97 recruits proteasomes to Insig-1 before extraction from membranes. *J. Biol. Chem.* **284:** 34889–34900.

18. Yam, P. C., and K. L. Knight. 2014. Generation of rabbit monoclonal antibodies. *Methods Mol. Biol.* **1131:** 71–79.

19. Wang, J., M. A. Mitsche, D. Lutjohann, J. C. Cohen, X. S. Xie, and H. H. Hobbs. 2015. Relative roles of ABCG5/ABCG8 in liver and intestine. *J. Lipid Res.* **56:** 319–330.

20. Wang, X., A. Spandidos, H. Wang, and B. Seed. 2012. PrimerBank: a PCR primer database for quantitative gene expression analysis, 2012 update. *Nucleic Acids Res.* **40:** D1144–D1149.

21. Sato, T., R. G. Vries, H. J. Snippert, M. van de Wetering, N. Barker, D. E. Stange, J. H. van Es, A. Abo, P. Kujala, P. J. Peters, et al. 2009. Single Lgr5 stem cells build crypt-villus structures in vitro without a mesenchymal niche. *Nature.* **459:** 262–265.

22. Brown, A. J., L. P. Sun, J. D. Feramisco, M. S. Brown, and J. L. Goldstein. 2002. Cholesterol addition to ER membranes alters conformation of SCAP, the SREBP escort protein that regulates cholesterol metabolism. *Mol. Cell.* **10:** 237–245.

23. Feil, R., J. Brocard, B. Mascrez, M. LeMeur, D. Metzger, and P. Chambon. 1996. Ligand-activated site-specific recombination in mice. *Proc. Natl. Acad. Sci. USA.* **93:** 10887–10890.

24. Madison, B. B., L. Dunbar, X. T. Qiao, K. Braunstein, E. Braunstein, and D. L. Gumucio. 2002. Cis elements of the villin gene control expression in restricted domains of the vertical (crypt) and horizontal (duodenum, cecum) axes of the intestine. *J. Biol. Chem.* **277:** 33275–33283.

25. Beutler, B., and A. Cerami. 1989. The biology of cachectin/TNF–a primary mediator of the host response. *Annu. Rev. Immunol.* **7:** 625–655.

26. Kirkland, D., A. Benson, J. Mirpuri, R. Pifer, B. Hou, A. L. DeFranco, and F. Yarovinsky. 2012. B cell-intrinsic MyD88 signaling prevents the lethal dissemination of commensal bacteria during colonic damage. *Immunity.* **36:** 228–238.

27. Scholzen, T., and J. Gerdes. 2000. The Ki-67 protein: from the known and the unknown. *J. Cell. Physiol.* **182:** 311–322.

28. Sato, R., J. Inoue, Y. Kawabe, T. Kodama, T. Takano, and M. Maeda. 1996. Sterol-dependent transcriptional regulation of sterol regulatory element-binding protein-2. *J. Biol. Chem.* **271:** 26461–26464.

29. Chen, G., G. Liang, J. Ou, J. L. Goldstein, and M. S. Brown. 2004. Central role for liver X receptor in insulin-mediated activation of Srebp-1c transcription and stimulation of fatty acid synthesis in liver. *Proc. Natl. Acad. Sci. USA.* **101:** 11245–11250.

30. Field, F. J., E. Born, S. Murthy, and S. N. Mathur. 2001. Regulation of sterol regulatory element-binding proteins in hamster intestine by changes in cholesterol flux. *J. Biol. Chem.* **276:** 17576–17583.

31. Kandutsch, A. A., and H. W. Chen. 1977. Consequences of blocked sterol synthesis in cultured cells. DNA synthesis and membrane composition. *J. Biol. Chem.* **252:** 409–415.

32. Field, F. J., E. Born, S. Murthy, and S. N. Mathur. 2001. Gene expression of sterol regulatory element-binding proteins in hamster small intestine. *J. Lipid Res.* **42:** 1–8.

33. Stange, E. F., and J. M. Dietschy. 1983. Cholesterol synthesis and low density lipoprotein uptake are regulated independently in rat small intestinal epithelium. *Proc. Natl. Acad. Sci. USA.* **80:** 5739–5743.

34. Stange, E. F., and J. M. Dietschy. 1983. Absolute rates of cholesterol synthesis in rat intestine in vitro and in vivo: a comparison of different substrates in slices and isolated cells. *J. Lipid Res.* **24:** 72–82.

35. Crouch, S. P., R. Kozlowski, K. J. Slater, and J. Fletcher. 1993. The use of ATP bioluminescence as a measure of cell proliferation and cytotoxicity. *J. Immunol. Methods.* **160:** 81–88.

36. Rawson, R. B., D. Cheng, M. S. Brown, and J. L. Goldstein. 1998. Isolation of cholesterol-requiring mutant Chinese hamster ovary cells with defects in cleavage of sterol regulatory element-binding proteins at site 1. *J. Biol. Chem.* **273:** 28261–28269.

37. Rawson, R. B., N. G. Zelenski, D. Nijhawan, J. Ye, J. Sakai, M. T. Hasan, T. Y. Chang, M. S. Brown, and J. L. Goldstein. 1997. Complementation cloning of S2P, a gene encoding a putative metalloprotease required for intramembrane cleavage of SREBPs. *Mol. Cell.* **1:** 47–57.

38. Adams, C. M., J. Reitz, J. K. De Brabander, J. D. Feramisco, L. Li, M. S. Brown, and J. L. Goldstein. 2004. Cholesterol and 25-hydroxycholesterol inhibit activation of SREBPs by different mechanisms, both involving SCAP and Insigs. *J. Biol. Chem.* **279:** 52772–52780.

39. Hannah, V. C., J. Ou, A. Luong, J. L. Goldstein, and M. S. Brown. 2001. Unsaturated fatty acids down-regulate SREBP isoforms 1a and 1c by two mechanisms in HEK-293 cells. *J. Biol. Chem.* **276:** 4365–4372.

40. Lee, J. N., X. Zhang, J. D. Feramisco, Y. Gong, and J. Ye. 2008. Unsaturated fatty acids inhibit proteasomal degradation of Insig-1 at a postubiquitination step. *J. Biol. Chem.* **283:** 33772–33783.

41. Engelking, L. J., G. Liang, R. E. Hammer, K. Takaishi, H. Kuriyama, B. M. Evers, W. P. Li, J. D. Horton, J. L. Goldstein, and M. S. Brown. 2005. Schoenheimer effect explained–feedback regulation of cholesterol synthesis in mice mediated by Insig proteins. *J. Clin. Invest.* **115:** 2489–2498.

42. Altmann, S. W., H. R. Davis, Jr., L. J. Zhu, X. Yao, L. M. Hoos, G. Tetzloff, S. P. Iyer, M. Maguire, A. Golovko, M. Zeng, et al. 2004. Niemann-Pick C1 Like 1 protein is critical for intestinal cholesterol absorption. *Science.* **303:** 1201–1204.

43. Stange, E. F., K. E. Suckling, and J. M. Dietschy. 1983. Synthesis and coenzyme A-dependent esterification of cholesterol in rat intestinal epithelium. Differences in cellular localization and mechanisms of regulation. *J. Biol. Chem.* **258:** 12868–12875.

44. Casteleyn, C., A. Rekecki, A. Van der Aa, P. Simoens, and W. Van den Broeck. 2010. Surface area assessment of the murine intestinal tract as a prerequisite for oral dose translation from mouse to man. *Lab. Anim.* **44:** 176–183.

45. Helander, H. F., and L. Fandriks. 2014. Surface area of the digestive tract – revisited. *Scand. J. Gastroenterol.* **49:** 681–689.

46. Ruzankina, Y., C. Pinzon-Guzman, A. Asare, T. Ong, L. Pontano, G. Cotsarelis, V. P. Zediak, M. Velez, A. Bhandoola, and E. J. Brown. 2007. Deletion of the developmentally essential gene ATR in adult mice leads to age-related phenotypes and stem cell loss. *Cell Stem Cell.* **1:** 113–126.

47. You, M., M. Fischer, M. A. Deeg, and D. W. Crabb. 2002. Ethanol induces fatty acid synthesis pathways by activation of sterol regulatory element-binding protein (SREBP). *J. Biol. Chem.* **277:** 29342–29347.

48. Shimomura, I., M. Matsuda, R. E. Hammer, Y. Bashmakov, M. S. Brown, and J. L. Goldstein. 2000. Decreased IRS-2 and increased SREBP-1c lead to mixed insulin resistance and sensitivity in livers of lipodystrophic and *ob/ob* mice. *Mol. Cell.* **6:** 77–86.

49. Kohjima, M., N. Higuchi, M. Kato, K. Kotoh, T. Yoshimoto, T. Fujino, M. Yada, R. Yada, N. Harada, M. Enjoji, et al. 2008. SREBP-1c, regulated by the insulin and AMPK signaling pathways, plays a role in nonalcoholic fatty liver disease. *Int. J. Mol. Med.* **21:** 507–511.

50. Sato, T., J. H. van Es, H. J. Snippert, D. E. Stange, R. G. Vries, M. van den Born, N. Barker, N. F. Shroyer, M. van de Wetering, and H. Clevers. 2011. Paneth cells constitute the niche for Lgr5 stem cells in intestinal crypts. *Nature.* **469:** 415–418.